# In-situ aggregation and early states of gelation of gold nanoparticle dispersions - Supplementary Information

Florian Schulz,[1,2] Avni Jain,[3,a)] Francesco Dallari,[3,b)] Verena Markmann,[3,c)] and Felix Lehmkühler[2,3]

[1)]*Institute of Nanostructure and Solid State Physics, University of Hamburg, Luruper Chaussee 149, 22761 Hamburg, Germany*

[2)]*The Hamburg Centre for Ultrafast Imaging, Luruper Chaussee 149, 22761 Hamburg, Germany*

[3)]*Deutsches Elektronen-Synchrotron DESY, Notkestr. 85, 22607 Hamburg, Germany*

(*Electronic mail: felix.lehmkuehler@desy.de)

(Dated: 20 March 2024)

[a)]Current address: Blue Yonder GmbH, Oberbaumbrücke 1, 20457 Hamburg, Germany.

[b)]Current address: University of Padua, Department of Physics and Astronomy, Via Marzolo 8, 35121 Padova, Italy.

[c)]Current address: Department of Physics, Technical University of Denmark, Kgs. Lyngby 2800, Denmark.

## I. INTENSITY $I(q)$

The azimuthally integrated intensities from run 1 and run 2 are shown in Fig. S1. These were used for the calculation of $S(q)$ as discussed in the main text. As for the $S(q)$, the different blue lines for run 2 correspond to different experimental times $t_w$ while keeping the temperature at 272 K.

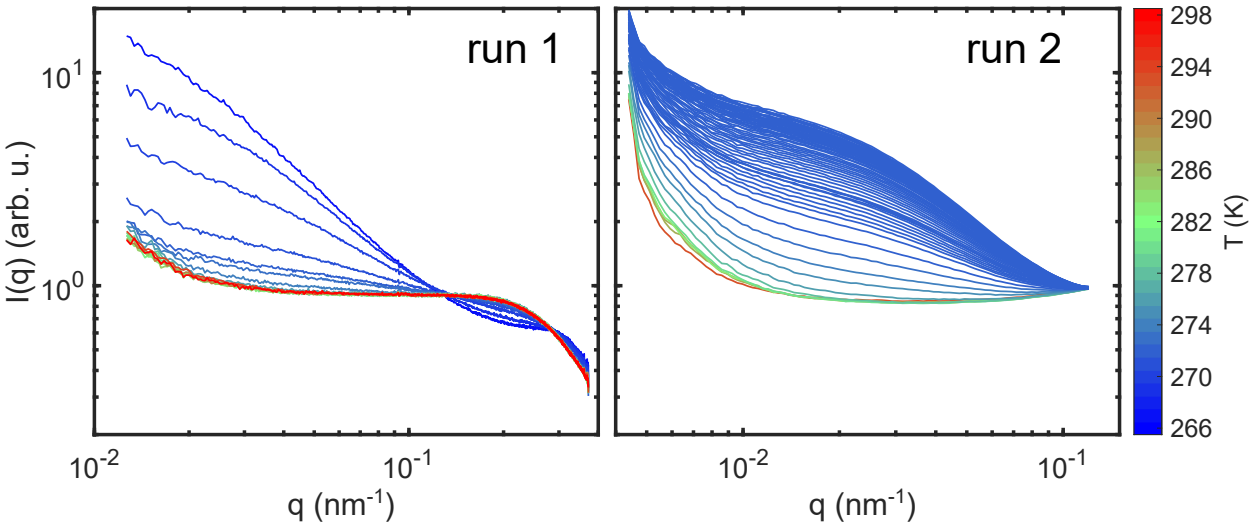


FIG. S1. Intensity $I(q)$ from run 1 (left) and run 2.

## II. STRUCTURE FACTOR

The structure factor $S(q)$ was obtained by $S(q,T) = I(q,T)/I(q,T_R)$ with room temperature $T_R$. This differs from the standard definition, where for spherical particles the intensity is divided by the form factor of the particles. However, at the particle concentration studied here, the difference between the form factor and the room temperature measurement is weak (see Fig. S2) which justifies our approach. Note that the form factor contribution to the scattering signal is dominated by the gold core which does not change significantly for the studied temperatures.

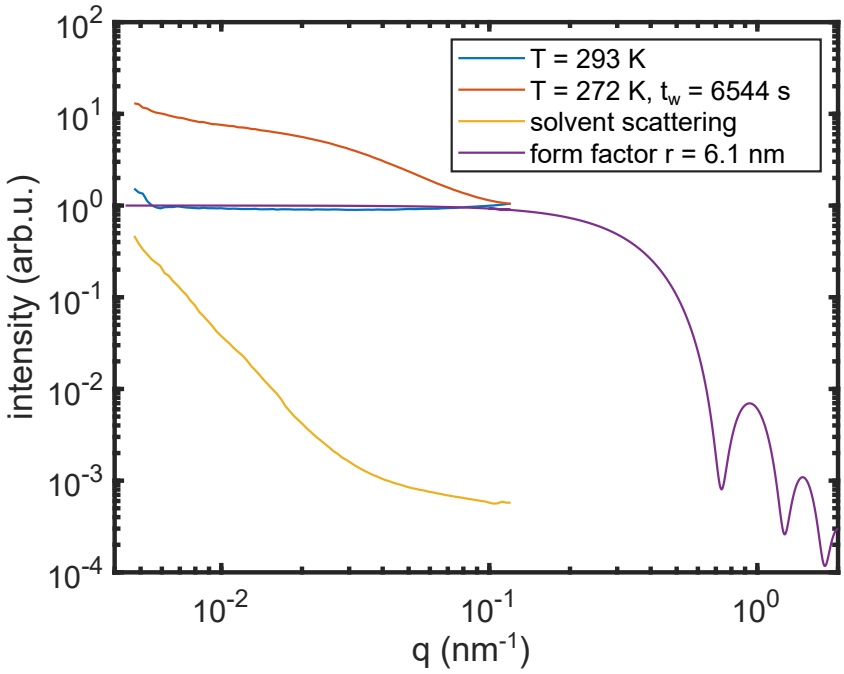


FIG. S2. Intensity from run 2 at 293 K used as form factor, compared to one dataset at 272 K, the contribution of solvent scattering and a calculated form factor with the size of the gold particles.

## III. RADIATION DAMAGE TESTS

The influence of the beam intensity on the structure and dynamics of the samples was investigated by measuring XPCS series at different transmission values using attenuators. The results on $I(q)$, $g_2$ and $\tau$ are shown in Fig. S3 from run 1 at $T = 276$ K. While using the full beam (transmission 1) results in beam damage visible by the change of $I(q)$ and changing baseline and shape in the $g_2$ functions, no significant effects can be seen at transmissions of 0.19 and below. For transmissions below about 1 % the counting statistics was not sufficient to extract relaxation times. Therefore, we used both transmissions of 0.19 and 0.036 for the data shown in the manuscript.

Note that the data of run 2 was measured typically at a transmission value of 0.02. In contrast to the data from run 1, an unfocused beam was used so that the photon density is additionally reduced by factor of about 100. This allowed us to take data from the same sample spots at different experimental times $t_w$ without any indication of beam-induced damage.

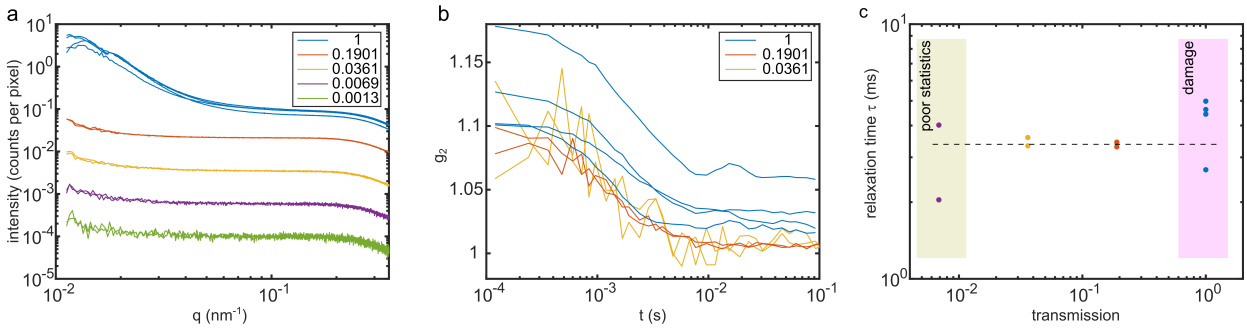


FIG. S3. Influence of beam transmission. (a) $I(q)$ from run 1 for five different transmission values as indicated in the legend. (b) Correlation function $g_2$ at $q = 0.045$ nm$^{-1}$ from run 1 for the three highest transmissions. (c) Relaxation times $\tau$ as function of transmission at $q = 0.045$ nm$^{-1}$. The dashed line marks the average of the two measurement at a transmission of 0.19.

## IV. Q-DEPENDENCE OF THE CORRELATION FUNCTION

The $q$-dependence of $g_2$ from run 2 are shown in Fig. S4 for three different experimental times and thus sample states. Here $|f(q,t)|^2 = (g_2 - 1)/\beta$ is shown to correct for small (statistical) variations of contrast $\beta$ with $q$. Note that the $q$-range that could be analyzed from run 1 is limited to two or three small $q's$.

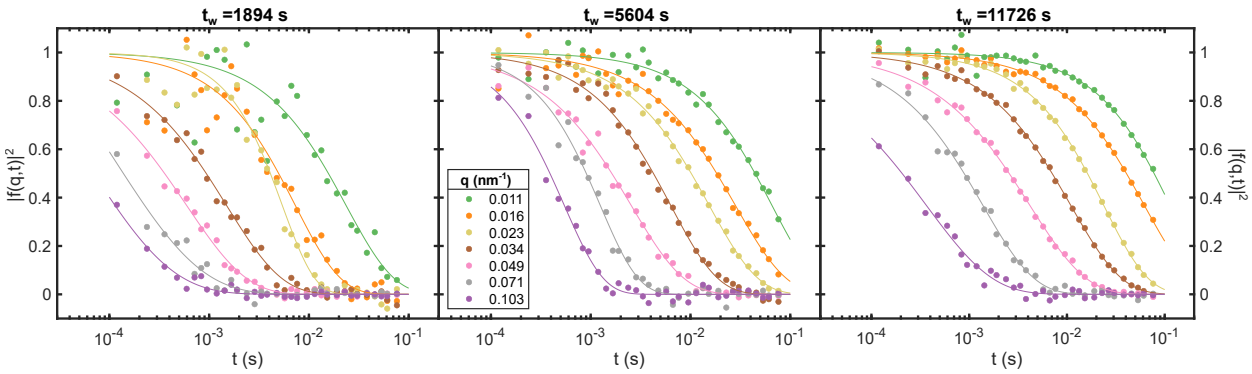


FIG. S4. Intermediate scattering function at different $q$-values for three experimental times $t_w$. The lines are fits to the KWW model (Eq. 2 in the manuscript).

## V. AGING

For run 1, the relaxation time was measured at different ages for temperatures below 272 K. For a quantitative comparison, we obtained an effective relaxation time after 1000 s age by fits to the data at various ages. The results of of the Arrhenius plots and fits are shown in Fig. S5 which represents a zoom to the same data shown in Fig. 2 of the main text.

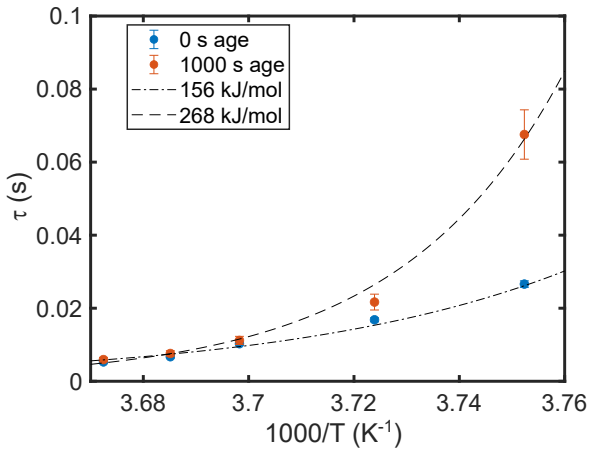


FIG. S5. Relaxation time $\tau$ as function of inverse temperature $T^{-1}$ for run 1 at $q = 0.045$ nm$^{-1}$ and for temperatures below 272 K. Dashed lines are Arrhenius fits as described in the main text.

## VI. RELAXATION TIMES AND KWW EXPONENTS

Fig. S6 shows the relaxation time for both runs at $q = 0.045$ nm$^{-1}$ as a function of the experimental time. These are compared to the KWW exponents $\gamma$ at the same $q$ that are found to be $\gamma \leq 1$ for all $t_w$. The onset of gelation is further characterized by a decrease of $\gamma$.

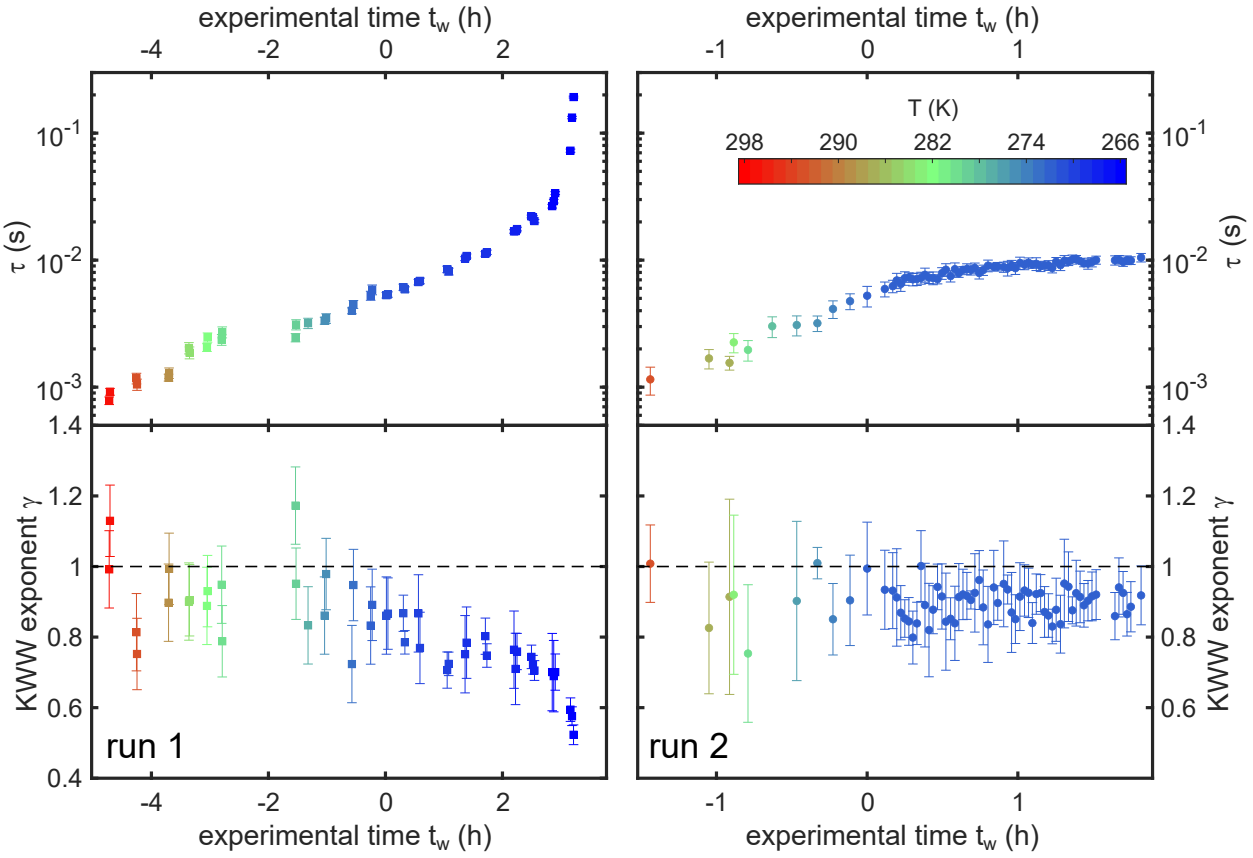


FIG. S6. Relaxation time $\tau$ (top) and KWW exponent $\gamma$ (bottom) at $q = 0.045$ nm$^{-1}$ as a function of experimental time $t_w$. Data measured in run 1 is shown left, results from run 2 right. The color of the data points refers to the temperature.

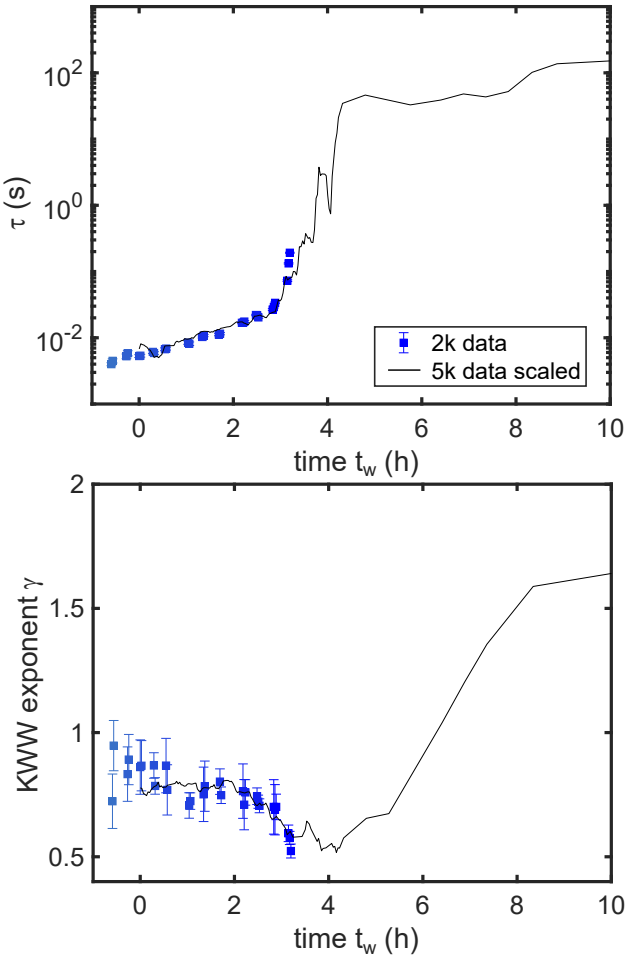


FIG. S7. Relaxation time $\tau$ (top) and KWW exponent $\gamma$ for $t_w \geq 0$ compared to results from Ref. 1. The latter data is corrected for the $q$-dependence of the dynamics (top) or shifted by 0.15 (bottom), their $t_w$-axis is scaled by a factor of 6.7 to match the current data.

Fig. S7 compares the relaxation times and KWW exponents for 2 kDa ligands (this study) with data from 5 kDa ligands[1]. Both data match when the 5 kDa is scaled by a factor 6.7, suggesting that also the system with shorter ligands transfers into a colloidal gel, but at slightly lower temperatures and longer times.

## VII. EFFECTIVE RADIUS

The effective radius has been calculated via the Stokes-Einstein model via $r_D = k_B T/(6\pi\eta D)$ for run 2 and is shown in Fig. S8.

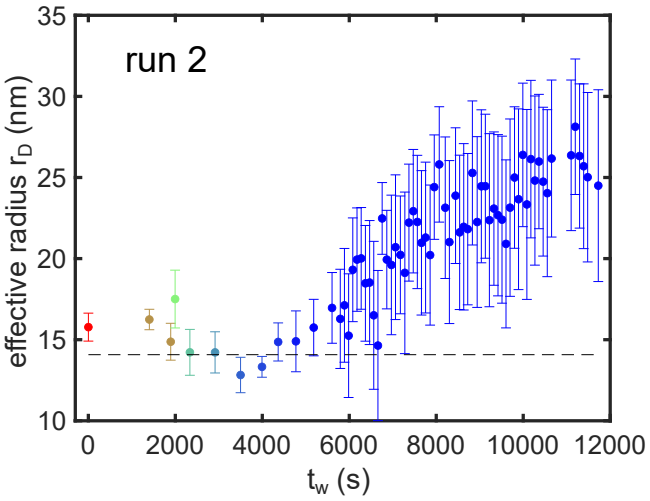


FIG. S8. Effective radius $r_D$ for run 2. The dashed line shows the equilibrium value of 14 nm.

## VIII. Q-DEPENDENCE OF SCATTERING INVARIANT

The scattering invariant

$$Q = \int_{q_{\min}}^{q_{\max}} q^2 I(q) \mathrm{d}q. \tag{1}$$

was calculated for the data taken in run 2 as a function of $q_{\max}$ up to 0.3 nm$^{-1}$. The results are shown in Fig. S9. Subfigure S9 a shows the invariant, subfigure S9 b the invariant normalized to the value at 298 K to compare the results for different $q_{\max}$. For $q_{\max} \geq 0.2$ nm$^{-1}$ the invariant is mostly constant for all temperatures.

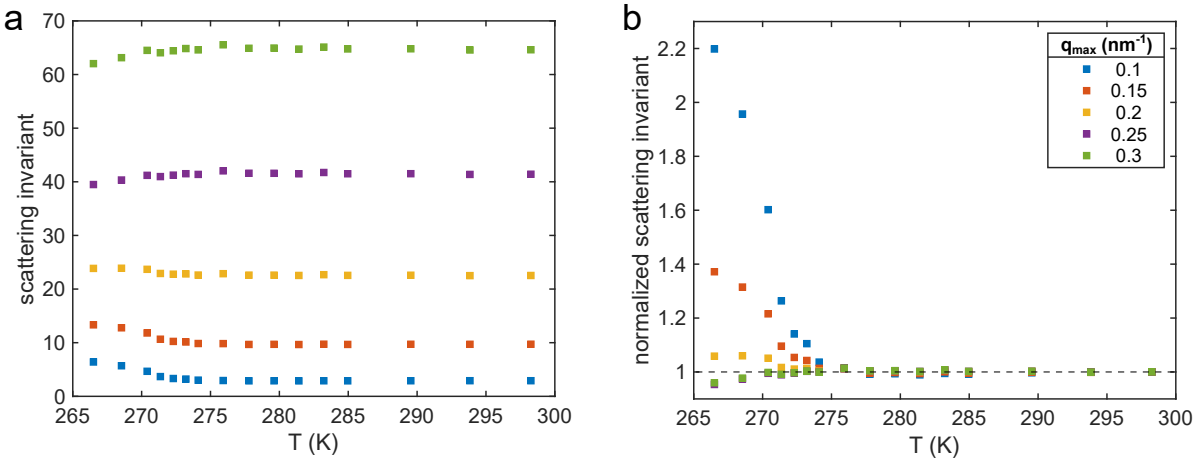


FIG. S9. (a) Scattering invariant for different values of $q_{\max}$ for run 1. (b) Scattering invariant normalized to the value at $T = 298$ K.

## REFERENCES

[1]A. Jain, F. Schulz, F. Dallari, V. Markmann, F. Westermeier, Y. Zhang, G. Grübel, and F. Lehmkühler, "Three-step colloidal gelation revealed by time-resolved x-ray photon correlation spectroscopy," J. Chem. Phys. **157**, 184901 (2022).